Hybrid Volitional Control of a Robotic Transtibial Prosthesis using a Phase Variable Impedance Controller

Ryan R. Posh[1], Jonathan A. Tittle[1], David J. Kelly[1], James P. Schmiedeler[1], and Patrick M. Wensing[1]

***Abstract*— For robotic transtibial prosthesis control, the global tibia kinematics can be used to monitor gait cycle progression and command smooth and continuous actuation. In this work, these global tibia kinematics define a phase variable impedance controller (PVIC), which is implemented as the nonvolitional base controller within a hybrid volitional control framework (PVI-HVC). The gait progression estimation and biomechanic performance of one able-bodied individual walking on a robotic ankle prosthesis via a bypass adapter are compared for three control schemes: benchmark passive controller, PVIC, and PVI-HVC. The different actuation of each had a direct effect on the global tibia kinematics, but the average deviation between the estimated and ground truth gait percentages were 1.6%, 1.8%, and 2.1%, respectively, for each controller. Both PVIC and PVI-HVC produced good agreement with able-bodied kinematic and kinetic references. As designed, PVI-HVC results were similar to those of PVIC when the user used low volitional intent, but yielded higher peak plantarflexion, peak torque, and peak power when the user commanded high volitional input in late stance. This additional torque and power also allowed the user to volitionally and continuously achieve activities beyond level walking, such as ascending ramps, avoiding obstacles, standing on tip-toes, and tapping the foot. In this way, PVI-HVC offers the kinetic and kinematic performance of the PVIC during level ground walking, along with the freedom to volitionally pursue alternative activities.**

I. Introduction

For individuals with transtibial amputation, robotic ankle prostheses could increase the mobility and quality of life compared to passive devices. While powered prosthetic hardware, as seen in Fig. 1, has seen major advances in recent decades, improving control of these devices remains essential to returning individuals to full ability. For cyclic tasks, such as walking, controllers can predict the desired joint position, torque, or impedance by estimating the progression of the gait cycle. The most traditional approach is to use a finite-state machine (FSM), which subdivides the gait cycle into discrete states that are navigated based on sensor-based transition rules. The discrete nature of FSM controllers leads to high repeatability, but also to an unnatural feel for users and the potential for state misclassification [1].

To avoid discontinuous actuation, gait cycle progression can be continuously estimated by monitoring a phase variable. A phase variable, denoted herein as ϕ, should progress monotonically from 0 to 100% of the gait cycle and can be used to define a unique, continuous relationship between sensor signals and joint actuation. Example phase variables include the foot center of pressure [2], [3] (only monitors gait progression in stance) and various hip and thigh kinematics [4], [5]. For transfemoral prostheses, thigh kinematics are preferred, as only sensors onboard the prosthesis are required. For transtibial prostheses, however, thigh-based phase variables require additional sensors on the user's body, increasing donning/doffing requirements. Therefore, a phase variable defined by the global tibia kinematics [6] is beneficial for transtibial prostheses since onboard sensors could measure it directly. The global tibia angle is measured in the sagittal plane relative to the gravity-fixed vertical.

For continuous impedance control, a desired stiffness, damping, and equilibrium angle must be predefined as functions of gait percentage. At each percentage of gait, multiple parameter combinations could yield the same joint torque, and ideal impedance trajectories remain an open research topic. Some have defined these trajectories via Parameter Dependent Lyapunov Functions [8], optimization techniques [9], [10], or heuristic linear definitions [11], while others have looked to empirically measure the parameters on the human body [12]. Some have worked to unify these findings [13], though consensus has not been fully reached.

While a smooth, continuous phase-based control approach can be applied to ambulation on level ground [2], ramps [14], and stairs [5], non-cyclic tasks such as standing on tip-toes, tapping the foot, or stepping side-to-side, require the incorporation of direct user intent. Direct myoelectric control (DMC) uses sensing of the lower leg muscle activity to provide users a direct sense of control and embodiment with the prosthetic ankle. DMC has shown promise in weight-

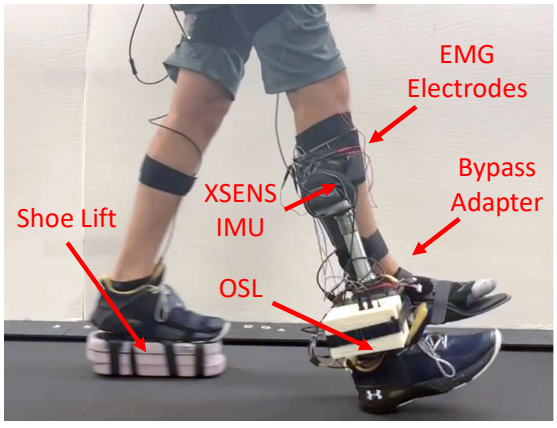

Fig. 1: Able-bodied user walked on Open-Source Leg (OSL) prosthesis via bypass adapter. User was outfitted with surface EMG electrodes and IMU from XSENS motion capture suit on tibia.

*This work was funded by NSF grants DGE-1841556 & CMMI-1943703.

[1]All authors are with the Department of Aerospace and Mechanical Engineering, University of Notre Dame, Notre Dame, IN 46556, USA rposh@nd.edu

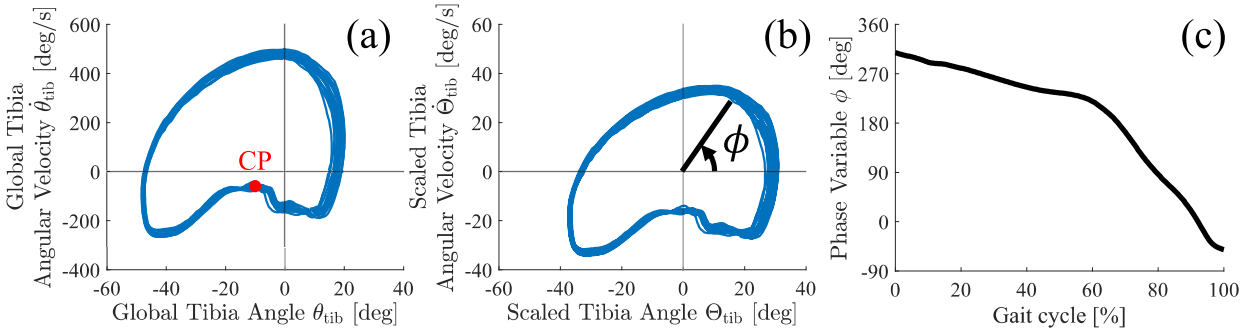

Fig. 2: Uncalibrated phase portrait with critical point CP (a) must be scaled and shifted (b) to produce monotonic relationship between phase variable and gait percentage (c) [7].

bearing activities, including walking [1], [15], [16], standing on tip-toes [1], [17], and perturbation reactions [18].

Hybrid Volitional Control (HVC) is a framework that combines standard walking controllers (such as FSM impedance control) with direct volitional controllers (such as DMC) [19]–[22]. When applied to the full gait cycle, HVC allows users to increase toe clearance in swing, modulate push-off power in stance, and perform non-cyclic activities by appropriately activating the instrumented muscles [1]. With the non-volitional base controller, HVC also allows users to walk on level ground with or without direct user input with reliable and cyclic control. Discrete transition-based controllers, however, may not be ideal as the non-volitional base controller within HVC due to potential interplay with the volitional component at transitions [1]. HVC has been combined with phase-variable control [22], though only in simulation. Therefore, this work introduces and assesses: 1) the first transtibial phase-variable impedance controller (PVIC) based on the global tibia kinematics; and 2) implementation of a hybrid volitional controller using PVIC (PVI-HVC). PVI-HVC is a promising way for individuals who have experienced transtibial amputation to smoothly achieve both cyclic and non-cyclic tasks of daily living.

II. Methods

A. Hardware

Each controller (passive, PVIC, and PVI-HVC) was implemented on the version 1 Open-Source Leg (OSL) [23], which has a range of motion of $\pm 15°$. All sensors were wired to a Raspberry Pi microcomputer, which received wireless commands from a remote laptop. For sensing, the OSL interfaced with two pressure sensors (SEN-08685; SparkFun Electronics), one each at the heel and toe, laid between two layers of polyurethane rubber compound (Vytaflex-60) and held in place by plastic 3D-printed contact plates. Each unit was secured to the bottom of the cosmetic footshell (LP Variflex®foot), which was itself enveloped by a shoe. The user donned the XSENS MVN Link motion capture suit for real-time measurement of the global tibia angle and angular velocity. Other data from the suit were used for lower body kinematic analysis offline. The XSENS suit communicated to the Raspberry Pi wirelessly via a private Wi-Fi router. One able-bodied user walked on the prosthesis via a bypass adapter (Fig. 1) with a contralateral shoe lift donned to accommodate leg length difference from the adapter. The user was outfitted with two surface electromyography (sEMG) amplifiers (SX230FW; Biometrics Ltd.), one each for the gastrocnemius (GAS) and tibialis anterior (TA). To avoid irritation or discomfort, thin ($\sim$1.25mm thickness), compliant medical-grade Ag/AgCl disk electrodes (TE/K50430-001, Technomed USA) interfaced with the user's skin. Hair was removed and the skin cleaned as necessary. Electrodes were aligned with the primary muscle fiber directions and wrapped with soft velcro straps for security.

B. Experimental Procedure

After all calibrations, the user performed four 30-second steady-state walking trials on a level treadmill at 0.8 m/s while holding a handrail. Trial 1 used a benchmark passive controller, and Trial 2 used PVIC. Trial 3 used PVI-HVC with relaxed muscles (low volitional user intent), and Trial 4 used PVI-HVC with maximal volitional contribution during push-off (high intent).

C. Benchmark Passive Controller

For calibration and a point of reference, a passive controller was implemented to mimic the behavior of a passive ankle-foot prosthesis. A constant impedance command was sent to the OSL with an ankle equilibrium angle set point of $0°$, a stiffness gain of 0.09 Nm/deg/kg, and a damping gain of 0.075 Nms/deg/kg.

D. Phase Variable Impedance Controller

As in [6], PVIC uses a global tibia-based phase variable. Calibration established the phase relationship between tibia kinematics and gait percentage, and a predefined impedance model was applied to achieve continuous impedance control.

1) Tibia-based Phase Variable: A phase portrait can be defined, as in Fig. 2a, with the tibia angular displacement (θ) on the horizontal axis and angular velocity ($\dot{\theta}$) on the vertical axis. In this phase portrait, heel strike occurs in the bottom right quadrant, where θ_{tib} is positive and $\dot{\theta}_{\text{tib}}$ is negative, and ϕ progresses clockwise from there through the gait cycle. To ensure a monotonic relationship between ϕ and gait percentage, θ_{tib} and $\dot{\theta}_{\text{tib}}$ are scaled and shifted with calibration constants x_0, y_0, and k as in Fig. 2b [7].

$$\Theta_{\text{tib}}(t) = \theta_{\text{tib}}(t) - x_0 \quad \text{and} \tag{1}$$

$$\dot{\Theta}_{\text{tib}}(t) = k(\dot{\theta}_{\text{tib}}(t) - y_0) \tag{2}$$

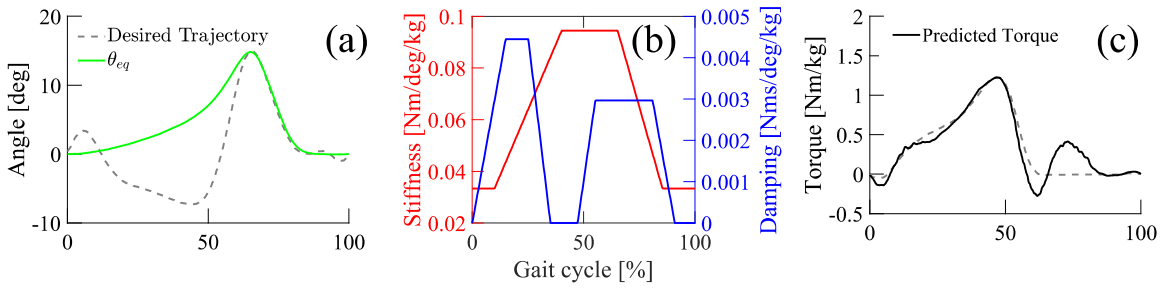

Fig. 3: Ankle equilibrium angle (a), ankle stiffness, and ankle damping (b) are continuous with respect to gait percentage. These parameters define impedance model to achieve predicted torque (c). Desired trajectories for ankle angle and torque (dashed lines) adapted from [24].

are then used to compute the final phase variable

$$\phi(t) = \text{atan2}(\dot{\Theta}_{\text{tib}}(t), \Theta_{\text{tib}}(t)). \tag{3}$$

As the gait cycle progresses from 0 to 100%, ϕ (starting between 270° and 360°) should monotonically decrease clockwise around the phase portrait until reaching the next heel strike (Fig. 2c).

2) Calibration: To determine the calibration parameters in Eqs. 1 and 2, the user walked at a steady-state speed of 0.8 m/s for 10-20 strides with the benchmark passive controller. During these strides, the global tibia angle and angular velocity were recorded, along with pressure sensor data. Heel strike, identified when heel pressure exceeds a predefined threshold, establishes a ground truth gait percentage by normalizing time between each heel strike. Critical Point Centering (CPC) calibration from [7] shifts the phase portrait based on its critical point where the global tibia angular velocity during stance is maximum (negative value in Fig. 2a). The parameters x_0, y_0, and k are chosen such that the average critical point is located on the y-axis $x_0 = \theta_{\text{tib}}(\max(\dot{\theta}_{\text{tib}_{\text{stance}}}))$, the phase portrait is vertically centered about the horizontal axis $y_0 = (\bar{\dot{\theta}}_{\text{tib}} + \underline{\dot{\theta}}_{\text{tib}})/2$, and the phase portrait is scaled such that the maxima/minima of θ_{tib} and $\dot{\theta}_{\text{tib}}$ are approximately equal

$$k = \frac{|\bar{\theta}_{\text{tib}} - \underline{\theta}_{\text{tib}}|}{|\bar{\dot{\theta}}_{\text{tib}} - \underline{\dot{\theta}}_{\text{tib}}|}.$$

Successful calibration yields a monotonic relationship between ground truth gait percentage and progression of ϕ, as in Fig. 2c. This relationship can then transform a desired impedance model expressed as a function of gait percentage to one expressed as a function of phase variable progression.

3) Impedance Model and Control: This work uses a heuristically defined impedance model that prioritizes a desired torque trajectory in stance and a desired position trajectory in swing, similar to the knee-ankle controller in [10]. It consists of desired trajectories for the ankle equilibrium angle, stiffness gain, and damping gain as functions of gait percentage, shown in Fig. 3. The equilibrium angle trajectory (Fig. 3a) during swing matches a scaled version of the desired able-bodied swing phase kinematics, beginning at the point of maximum plantarflexion. The able-bodied reference was adapted from [24], but the maximum plantarflexion angle was scaled down from approximately 20° to match

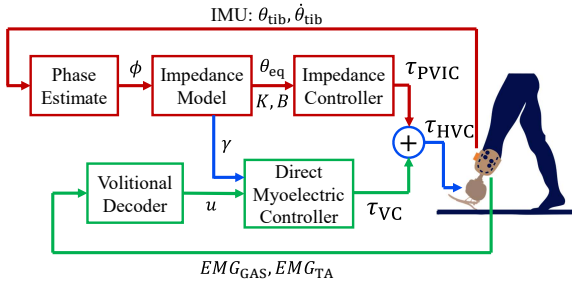

Fig. 4: Hybrid volitional control (HVC, blue) is an additive combination of torque from phase variable impedance control (PVIC, red) and volitional control (VC, green).

the OSL's plantarflexion limit of 15°. The equilibrium angle trajectory during stance was defined such that the difference between the desired able-bodied kinematics and the equilibrium angle could be linearly scaled to match the desired ankle torque. This was achieved via a simply defined stiffness trajectory that linearly increased during mid-stance as in [12], remained constant during push-off, and linearly decreased in late swing to ensure that the values at 0% and 100% of gait were equal for continuity across heel strike (Fig. 3b). The heuristically defined damping trajectory consists of two peaks, as observed in [12], one that assists with shock absorption in early stance and the other that dampens the position tracking in swing to reduce any oscillations related to overshoot (Fig. 3b).

As outlined in Fig. 4, measuring the phase variable progression enables a continuous estimate of gait percentage so that the desired stiffness, damping, and equilibrium angle can be applied. The output torque then is

$$\mathcal{T}_{\text{PVIC}} = -K(\theta_{\text{ankle}} - \theta_{\text{eq}}) - B\dot{\theta}_{\text{ankle}}, \tag{4}$$

where the stiffness K, damping B, and ankle equilibrium angle θ_{eq} are predefined functions of gait percentage, and, after calibration, also functions of the phase variable ϕ. Using able-bodied kinematics for reference, the expected torque from this impedance model is shown in Fig. 3c. The poor agreement between desired and predicted torque during the swing phase in Fig. 3c exists only in our analysis of applying these damping profiles to fixed kinematic data. In hardware, since the damping affects kinematic trajectories, this discrepancy does not persist.

E. Phase Variable Impedance Hybrid Volitional Controller

As outlined in [22], HVC sums the torque contributions from a non-volitional base component (NVBC) and a vo-

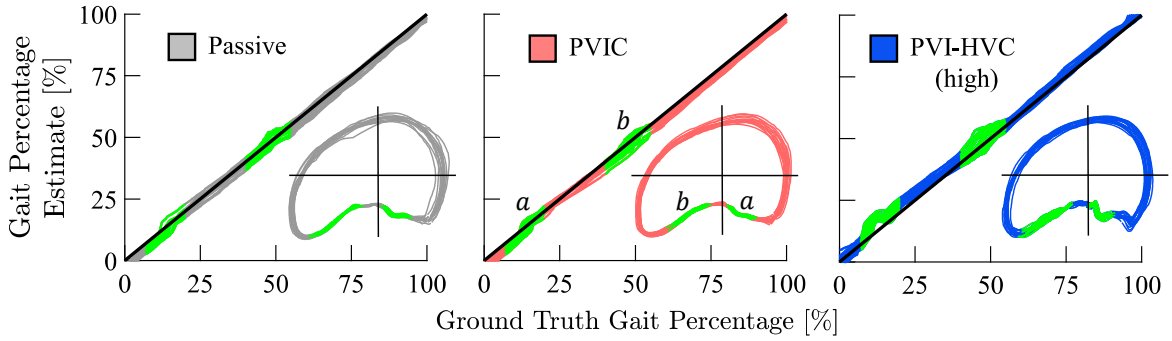

Fig. 5: Measurement of scaled phase portrait leads to gait percentage estimation for passive control (grey), PVIC (red), and PVI-HVC with high intent (darker blue). Highlighted in green are regions of increased prediction error with corresponding locations *a* and *b*.

litional component. With PVIC (Sec. II-D) serving as the NVBC, the output torque is

$$\tau_{\mathrm{PVI-HVC}} = \tau_{\mathrm{PVIC}} + \tau_{\mathrm{VC}}. \tag{5}$$

In this way, users can rely on the NVBC to walk naturally and reliably on level ground without the need to use any volitional input, but can also volitionally contribute at any time to achieve non-standard activities, navigate obstacles or uneven terrain, or increase the torque and power of the NVBC when walking, if desired.

The volitional component follows [1] and converts GAS and TA sEMG signals to a single volitional input variable,

$$u = \begin{cases} \sqrt{u_p^2 + u_d^2} \cdot \left(\frac{m - m_0}{m_{\mathrm{GAS}} - m_0}\right) & \text{if } m \geq m_0 \\ -\sqrt{u_p^2 + u_d^2} \cdot \left(\frac{m - m_0}{m_{\mathrm{TA}} - m_0}\right) & \text{if } m < m_0 \end{cases}, \tag{6}$$

$$u_p = \mathrm{EMG}_{\mathrm{GAS}}/\mathrm{MVA}_{\mathrm{GAS}}, \tag{7}$$

$$u_d = \mathrm{EMG}_{\mathrm{TA}}/\mathrm{MVA}_{\mathrm{TA}}, \tag{8}$$

$$m = u_p/u_d, \tag{9}$$

$$m_0 = \mathrm{atan}\left(\tan(m_{\mathrm{GAS}}) + \tan(m_{\mathrm{TA}})/2\right), \tag{10}$$

where u_p (plantarflexion) and u_d (dorsiflexion) are the GAS and TA sEMG inputs, each normalized by its maximum voluntary activation (MVA) level, m is the real-time co-contraction slope, and m_{GAS} and m_{TA} are average co-contraction slopes measured when the user attempts to strictly plantar- or dorsiflex, respectively. $\mathrm{MVA}_{\mathrm{GAS}}$, $\mathrm{MVA}_{\mathrm{TA}}$, m_{GAS}, m_{TA}, and bisector m_0 are found during volitional calibration to define the volitional decoder in Fig. 4 and Eq. 6. The $\sqrt{u_p^2 + u_d^2}$ term is constrained to never exceed unity, and m is constrained to never be larger than m_{GAS} or smaller than m_{TA}. Therefore, the volitional input u ranges from 1 for maximum plantarflexion intent to -1 for maximum dorsiflexion intent.

The volitional component was calibrated according to [25]. The user performed 5 maximum voluntary isometric contractions for plantarflexion and dorsiflexion (maxima defining $\mathrm{MVA}_{\mathrm{GAS}}$ and $\mathrm{MVA}_{\mathrm{TA}}$). Co-contraction parameters were found via a dynamic calibration in which the user walked on the treadmill for 30 seconds using the benchmark passive controller. m_{GAS} was calculated as the average slope m for conditions when $u_p > 0.5$ and $u_d < 0.5$, and m_{TA} as the average slope when $u_p < 0.5$ and $u_d > 0.5$. Ultimately, the torque from the volitional component is

$$\tau_{\mathrm{VC}} = K(|\theta_{\mathrm{eq}}| - \theta_{\mathrm{max}})u, \tag{11}$$

where θ_{max} is the maximum plantarflexion angle of the prosthesis (15°) and K and θ_{eq} are the stiffness and equilibrium angle, respectively, defined by the impedance model in Sec II-D.3. When combined with the PVIC, this control acts to volitionally modulate the equilibrium angle up to the maximum range of the prosthesis.

F. Data Processing

The OSL's motor encoder measured the motor position, which was mapped to the ankle angle via the OSL's four-bar mechanism kinematics [23]. The sensed motor current was converted to motor torque and combined with the four-bar kinematics to estimate ankle torque. The prosthetic ankle joint power was computed from these quantities. The sEMG sensors feature a band-pass filter between 20 and 460 Hz and 1000x amplification. The system operated at 220 Hz (limited by the XSENS suit communication), with the rectified sEMG signals, pressure sensor signals, and global tibia velocity filtered with moving average filters defined by 300 ms, 60 ms, and 70 ms windows, respectively. By smoothing the velocity, the phase portrait is slightly tilted due to a small delay between global tibia angle and angular velocity. Per [6], the physical meanings of the phase portrait axes are unimportant in steady-state activities provided the inputs uniquely correspond to the desired gait percentage. The data were divided into strides based on heel strike occurrences. No strides were removed as outliers.

III. Results & Discussion

A. Steady State Phase Estimation

Figure 5 shows the scaled phase portrait and gait percentage estimates for all recorded strides when walking with passive control, PVIC, and PVI-HVC with high intent. As more actuation is introduced into the control, the tibia kinematics, and thus the phase variable and estimated gait percentage, are increasingly affected at particular locations. Shown in Table I, the maximum errors in gait percentage estimate were 4.8% for passive (at 55.6% of gait), 4.7% for PVIC (at 8.1%), and 8.3% (at 44.8%) for PVI-HVC. These larger deviations around 10% and 50% of gait, highlighted in

Fig. 5, correspond to ϕ values near $290°$ and $235°$ in Fig. 2c. At these locations, the near zero slope of the relationship means that small changes in ϕ correspond to large changes in estimated gait percentage. Despite these localized errors, the average errors in gait percentage estimate across the full stride were 1.6%, 1.8%, and 2.1% for passive, PVIC, and PVI-HVC, respectively (Table I).

B. Biomechanic Performance

Figure 6 shows results of the 30-second steady-state treadmill walking trials with the 3 controllers: passive control (18 strides), PVIC (16 strides), and PVI-HVC with both low (16 strides) and high (17 strides) user intent. Each plot is the average trajectory $\pm$ 2 standard deviations, and desired able-bodied trajectories are shown for reference. The expected power trajectory is the product of the desired torque and the time derivative of the desired angle.

1) Ankle Kinematics: The ankle angle trajectory generated by the passive controller shows natural dorsiflexion in stance due to loading conditions, but no significant plantarflexion related to toe-off, resulting in a root-mean-squared error (RMSE) from the desired trajectory of $5.1°$. With an equilibrium angle of $0°$, the ankle remains neutral in the absence of ground reaction forces in swing, and the constant damping gain reduces oscillations during the stance-to-swing transition. PVIC generated a smooth, continuous, and repeatable ankle angle trajectory, with an RMSE of $2.2°$ and an average peak plantarflexion angle of $12.5°$. Slightly less dorsiflexion than desired is observed in stance, likely due to the atypical loading conditions associated with walking with a bypass adapter and holding the treadmill handrail.

As expected, PVI-HVC with low intent showed similar performance to PVIC (RMSE of $2.9°$). Oscillations and variance around heel strike increased, and dorsiflexion in stance decreased, all attributed to the baseline volitional input, as observed in Fig. 6, from the unintentional muscle activation involved in walking with low intent. PVI-HVC with high user intent similarly generated less dorsiflexion in early stance, but the user was able to volitionally command a large plantarflexion intent between 40 and 75% of gait to exceed the desired peak plantarflexion angle on average. PVI-HVC showed the highest stride-to-stride variation due to the variability of human input. Overall, the ankle angle RMSE of PVI-HVC with high intent was $4.3°$.

2) Ankle Kinetics: Despite an inability to track the desired ankle kinematics, the passive controller produced a smooth and natural torque trajectory qualitatively similar to, but quantitatively less than the desired torque trajectory, with an RMSE of 0.25 Nm/kg. Peak power, however, reached only 26% of the desired on average (Table I). Again, PVIC produced a smooth and repeatable torque trajectory that was close to the desired (RMSE of 0.18 Nm/kg). A smaller plantarflexion moment was observed in stance, consistent with a reduction in the dorsiflexion angle related to loading. The max power generated was 1.07 W/kg on average. As expected, PVI-HVC generated very similar torque (RMSE of 0.17 Nm/kg) and power (peak of 1.26 W/kg) trajectories to PVIC when volitional input remained low. PVI-HVC with high intent produced torque and power trajectories more similar to the desired, with a maximum plantarflexion moment of 1.50 Nm/kg and a maximum power of 2.01 W/kg. PVC-HVC with high intent produced the least kinetic error from desired, with RMS torque and power errors of 0.17 Nm/kg and 0.25 W/kg, respectively.

TABLE I: Overall Controller Performance Results

	AB	Passive	PVIC	PVI-HVC (low)	PVI-HVC (high)
Avg. Gait % Error [%]	-	1.6	1.8	1.82	2.1
Max Gait % Error [%]	-	4.8	4.7	5.39	8.3
Avg. Angle RMSE [degs]	-	5.28	2.81	2.52	3.67
Avg. Torque RMSE [Nm/kg]	-	0.25	0.18	0.17	0.17
Avg. Peak Torque [Nm/kg]	1.23	0.72	0.96	1.01	1.6
Avg. Peak Power [W/kg]	1.94	0.50	1.10	1.30	2.00

C. Volitional Activities

By contributing volitional input when desired, the user achieved activities beyond level ground walking, including standing on tip-toes, tapping the foot, ascending a ramp, and avoiding obstacles in swing (Fig. 7 and supplemental video). This is a major advantage of the PVI-HVC framework. When the tibia segment remains relatively static, the controller approximates a DMC implementation.

D. Controller Strengths & Study Limitations

To the authors' knowledge, this is the first implementation on an ankle prosthesis of a phase-variable impedance controller using a tibia-based phase variable. This PVIC not only offers high accuracy gait estimation, but also well matches, both qualitatively and quantitatively, intact ankle kinematics and kinetics for level ground walking. Adding myoelectric volitional input to the system in PVI-HVC extends this controller to one that also enables activities of daily living beyond level ground walking. Unlike HVC with an FSM non-volitional base controller [1], this continuous controller did not exhibit unexpected behaviors from the interactions between the PVIC and the volitional component.

A limitation of this study is the relatively small range of ankle motion of the OSL, which only allows for proper comparisons to slow able-bodied walking. By modifying the impedance model, this framework can easily be extended to other hardware platforms with wider ranges of ankle motion. Additionally, the data in this study come from only one able-bodied user, and the effects on biomechanic performance of walking on the prosthesis via a bypass adapter are non-trivial. Future work will assess the performance of these controllers with multiple subjects with transtibial amputation.

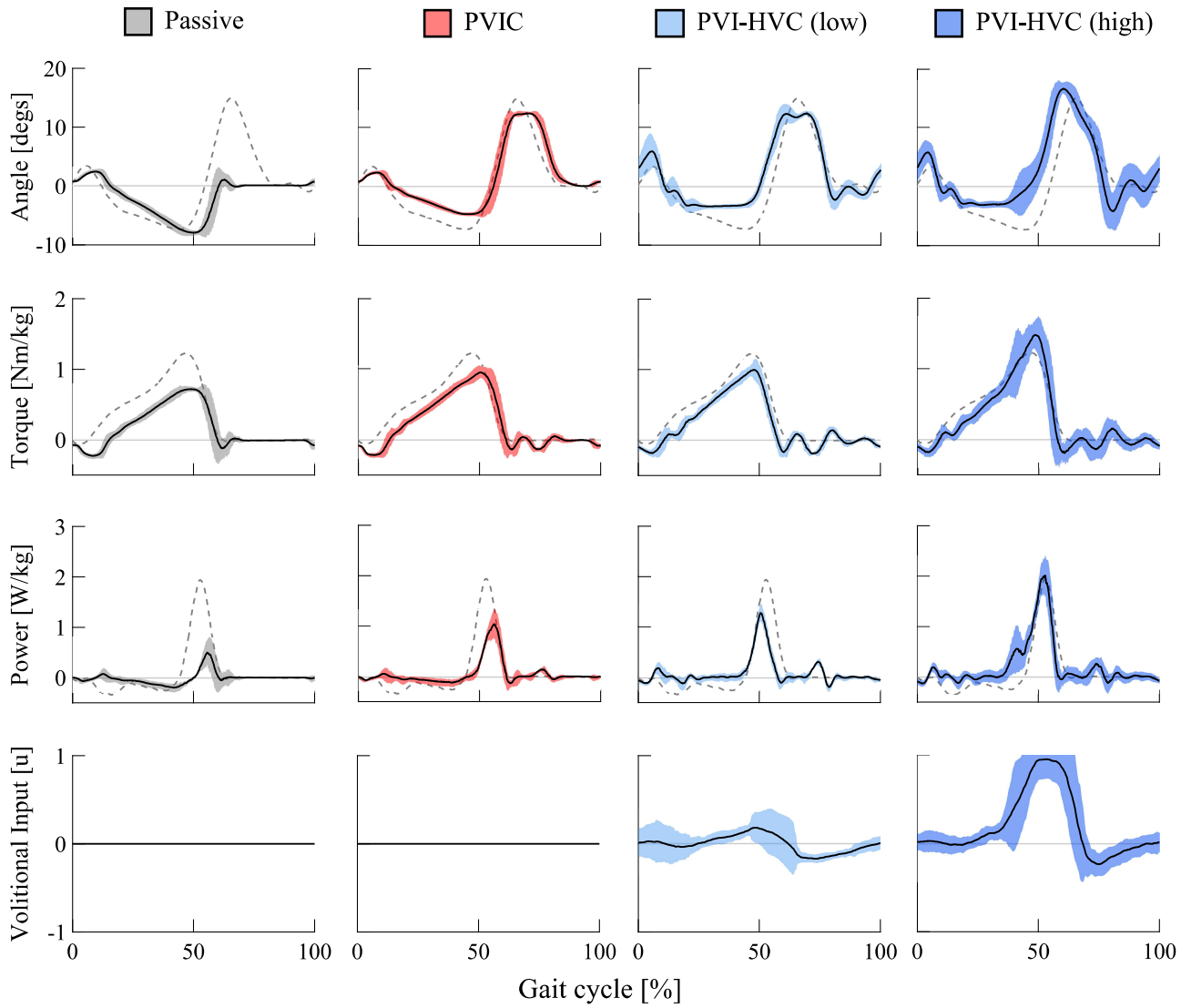

Fig. 6: Mean prosthesis ankle angle, normalized torque, normalized power, and volitional input versus gait cycle percentage were measured for passive control (grey), PVIC (red), PVI-HVC with low intent (lighter blue), and PVI-HVC with high intent (darker blue). Each plot shows average trajectory $\pm$ 2 standard deviations. Desired trajectories (dashed grey) were adapted from able-bodied walking [24].

Fig. 7: With volitional input, users can stand on tip-toes, ascend ramps, avoid obstacles, and perform other activities (see supplemental video).

IV. Conclusion

This paper presents the first phase-variable impedance controller (PVIC) based on the global tibia kinematics and employs this controller in a hybrid volitional control framework (PVI-HVC) to achieve both cyclic and non-cyclic tasks. In comparisons among a baseline passive controller, PVIC implemented alone, and PVI-HVC, the different actuation associated with each had a direct effect on the gait percentage estimation at certain stages of gait. The gait percentage predictions when using each of the three, though, had an average accuracy of approximately 2%. For level ground walking, PVIC approximated the kinematic and kinetic performance of an intact ankle very well. PVI-HVC with low user volitional input retained the performance of PVIC, while adding high volitional input within PVI-HVC increased the plantarflexion, peak torque, and peak power when walking, resulting in the best agreement to able-bodied torque and power references. Beyond level walking, PVI-HVC also makes it possible to achieve activities such as slope walking, obstacle avoidance, and tip-toe standing.

REFERENCES

[1] R. R. Posh, J. P. Schmiedeler, and P. M. Wensing, "Finite-state impedance and direct myoelectric control for robotic ankle prostheses: Comparing their performance and exploring their combination," *IEEE T Neur Sys Reh*, vol. 31, pp. 2778–2788, 2023.

[2] R. D. Gregg, T. Lenzi, N. P. Fey, L. J. Hargrove, and J. W. Sensinger, "Experimental effective shape control of a powered transfemoral prosthesis," *IEEE Int Conf Rehabil Robot*, pp. 1–7, 2013.

[3] R. D. Gregg and J. W. Sensinger, "Towards biomimetic virtual constraint control of a powered prosthetic leg," *IEEE T Control Syst Technol*, vol. 22, no. 1, pp. 246–254, 2013.

[4] D. J. Villarreal and R. D. Gregg, "A survey of phase variable candidates of human locomotion," *IEEE Int Conf Eng Med Biol Soc*, pp. 4017–4021, 2014.

[5] R. J. Cortino, E. Bolívar-Nieto, T. K. Best, and R. D. Gregg, "Stair ascent phase-variable control of a powered knee-ankle prosthesis," in *IEEE Int Conf Intell Robots Syst*, 2022, pp. 5673–5678.

[6] M. A. Holgate, T. G. Sugar, and A. W. Bohler, "A novel control algorithm for wearable robotics using phase plane invariants," in *IEEE Int Conf Robot Autom*, 2009, pp. 3845–3850.

[7] R. R. Posh, J. A. Tittle, J. P. Schmiedeler, and P. M. Wensing, "Calibration of a tibia-based phase variable for control of robotic transtibial prostheses," in *IEEE Int Conf Intell Robots Syst (to appear)*, 2023.

[8] A. Mohammadi and R. D. Gregg, "Variable impedance control of powered knee prostheses using human-inspired algebraic curves," *J Comput Nonlinear Dyn*, vol. 14, no. 10, 2019.

[9] Y. Hu and K. Mombaur, "Analysis of human leg joints compliance in different walking scenarios with an optimal control approach," *IFAC-PapersOnLine*, vol. 49, no. 14, pp. 99–106, 2016.

[10] T. K. Best, C. G. Welker, E. J. Rouse, and R. D. Gregg, "Data-driven variable impedance control of a powered knee–ankle prosthesis for adaptive speed and incline walking," *IEEE Transactions on Robotics*, 2023.

[11] W. Hong, V. Paredes, K. Chao, S. Patrick, and P. Hur, "Consolidated control framework to control a powered transfemoral prosthesis over inclined terrain conditions," in *IEEE Int Conf Robot Autom*, 2019, pp. 2838–2844.

[12] H. Lee, E. J. Rouse, and H. I. Krebs, "Summary of human ankle mechanical impedance during walking," *IEEE J Transl Eng He*, vol. 4, pp. 1–7, 2016.

[13] N. A. Kumar, W. Hong, and P. Hur, "Impedance control of a transfemoral prosthesis using continuously varying ankle impedances and multiple equilibria," in *IEEE Int Conf Robot Autom*, 2020, pp. 1755–1761.

[14] T. K. Best, K. R. Embry, E. J. Rouse, and R. D. Gregg, "Phase-variable control of a powered knee-ankle prosthesis over continuously varying speeds and inclines," in *IEEE Int Conf Intell Robots Syst*, 2021, pp. 6182–6189.

[15] S. Huang, J. P. Wensman, and D. P. Ferris, "Locomotor adaptation by transtibial amputees walking with an experimental powered prosthesis under continuous myoelectric control," *IEEE T Neur Sys Reh*, vol. 24, no. 5, pp. 573–581, 2015.

[16] L. J. Hargrove, A. M. Simon, A. J. Young, R. D. Lipschutz, S. B. Finucane, D. G. Smith, and T. A. Kuiken, "Robotic leg control with EMG decoding in an amputee with nerve transfers," *N Engl J*, vol. 369, no. 13, pp. 1237–1242, 2013.

[17] C. Shah, A. Fleming, V. Nalam, M. Liu, and H. H. Huang, "Design of emg-driven musculoskeletal model for volitional control of a robotic ankle prosthesis," in *IEEE Int Conf Intell Robots Syst*, 2022, pp. 12 261–12 266.

[18] A. Fleming and H. H. Huang, "Proportional myoelectric control of a powered ankle prosthesis for postural control under expected perturbation: A pilot study," in *IEEE Int Conf Rehabil Robot*, 2019, pp. 899–904.

[19] C. D. Hoover, G. D. Fulk, and K. B. Fite, "Stair ascent with a powered transfemoral prosthesis under direct myoelectric control," *IEEE-ASME T Mech*, vol. 18, no. 3, pp. 1191–1200, 2012.

[20] J. Wang, O. A. Kannape, and H. M. Herr, "Proportional EMG control of ankle plantar flexion in a powered transtibial prosthesis," in *IEEE Int Conf Rehabil Robot*, 2013, pp. 1–5.

[21] B. Chen and Q. Wang, "Combining human volitional control with intrinsic controller on robotic prosthesis: A case study on adaptive slope walking," in *Conf Proc IEEE Eng Med Biol Soc*, 2015, pp. 4777–4780.

[22] R. R. Posh, J. P. Schmiedeler, and P. M. Wensing, "Hybrid volitional control as a framework for lower-limb prosthetic control: A simulation study," in *IEEE Int Conf Intell Robots Syst*, 2021, pp. 6167–6163.

[23] A. F. Azocar, L. M. Mooney, L. J. Hargrove, and E. J. Rouse, "Design and characterization of an open-source robotic leg prosthesis," in *IEEE Int Conf Biomed Robot Biomechatron*, 2018, pp. 111–118.

[24] D. A. Winter, "Biomechanical motor patterns in normal walking," *J Mot Behav*, vol. 15, no. 4, pp. 302–330, 1983.

[25] R. R. Posh, E. C. Barry, J. P. Schmiedeler, and P. M. Wensing, "Lower-limb myoelectric calibration postures for transtibial prostheses," *IEEE T Neur Sys Reh (to appear)*, 2024.